False spin zeros in the angular dependence of magnetic quantum oscillations in quasi-two-dimensional metals

P. D. Grigoriev*
L. D. Landau Institute for Theoretical Physics, 142432 Chernogolovka, Russia;
National University of Science and Technology "MISiS," Moscow 119049, Russia;
P.N. Lebedev Physical Institute, RAS, Moscow 119991, Russia;
and Institut Laue-Langevin, Boîte Postale 156, 41 avenue des Martyrs, 38042 Grenoble Cedex 9, France

T. I. Mogilyuk
National Research Centre "Kurchatov Institute," Moscow, Russia
(Received 14 February 2017; published 15 May 2017)

The interplay between angular and quantum magnetoresistance oscillations in quasi-two-dimensional metals leads to the angular oscillations of the amplitude of quantum oscillations. This effect becomes pronounced in high magnetic field, where the simple factorization of the angular and quantum oscillations is not valid. The amplitude of quantum magnetoresistance oscillations is reduced at the Yamaji angles, i.e., at the maxima of the angular magnetoresistance oscillations. These angular beats of the amplitude of quantum oscillations resemble and may be confused with the spin-zero effect, coming from the Zeeman splitting. The proposed effect of "false spin zeros" becomes stronger in the presence of incoherent channels of interlayer electron transport and can be used to separate the different contributions to the Dingle temperature and to check for violations of the standard factorization of angular and quantum magnetoresistance oscillations.

DOI: 10.1103/PhysRevB.95.195130

I. INTRODUCTION

Layered quasi-two-dimensional (Q2D) compounds are of great interest to modern condensed-matter physics and comprise almost all high-temperature superconductors, organic metals, intercalated graphites, GaAs layered heterostructures, rare-earth tellurides, and numerous other natural and artificial layered conductors. The magnetic quantum oscillations (MQOs) and angular dependence of magnetoresistance (MR) are two traditional and common tools to probe the electronic structure of metals [1–3]. In Q2D metals even the classical MR shows oscillating behavior as a function of tilt angle θ of magnetic field with respect to the normal to conducting layers [4,5], called the angular magnetoresistance oscillations (AMROs). Now, together with MQOs, AMROs are extensively used to study the electronic structure in layered organic metals (see, e.g., [6–12] for reviews), heterostructures [13], ruthenates [14], tungsten bronze [15], and even cuprate high-temperature superconductors [16–21].

The Fermi surface in Q2D metals has the shape of a warped cylinder, which corresponds to the strongly anisotropic electron dispersion

$$\epsilon_{3D}(\mathbf{k}) \approx \epsilon_{2D}(k_x, k_y) - 2t_z \cos(k_z d), \tag{1}$$

where $\hbar\{k_x, k_y, k_z\}$ are the electron momentum components, $\hbar$ is Planck's constant, d is the interlayer distance, and the interlayer transfer integral t_z is much less than the Fermi energy E_F. In some cases, especially in low-symmetry crystals, $t_z = t_z(k_x, k_y)$ depends on in-plane momentum, which affects AMROs and MQOs [22–25]. However, to describe most compounds it is sufficient to take $t_z(k_x, k_y) \approx$ const. The geometrical explanation of AMROs [5] for the electron dispersion in Eq. (1) is based on the observation that for the quadratic and isotropic in-plane electron dispersion $\epsilon_{2D}(k_x,k_y) = \hbar^2(k_x^2 + k_y^2)/2m^*$ and for $t_z \approx$ const the cross-section areas of such a warped cylindrical Fermi surface in the first order in t_z become independent of k_z for some tilt angles $\theta = \theta_{\text{Yam}}$ of magnetic field, now called the Yamaji angles [6–12]. The Yamaji angles give the minima of the angular dependence of interlayer conductivity $\sigma_{zz}(\theta)$ and correspond to the zeros of the Bessel function $J_0(\kappa)$, where $\kappa \equiv k_F d \tan\theta$ and k_F is the in-plane Fermi momentum. The direct calculation of interlayer conductivity from the Boltzmann transport equation in the τ approximation with the electron dispersion in Eq. (1) gives [26]

$$\frac{\sigma_{zz}(\theta)}{\sigma_{zz}} = [J_0(\kappa)]^2 + 2\sum_{\nu=1}^{\infty} \frac{[J_\nu(\kappa)]^2}{1 + (\nu\omega_c\tau)^2} \equiv \Phi_{\text{AMRO}}(\theta), \tag{2}$$

where τ is the electron mean free time and the cyclotron frequency ω_c in Q2D metals depends on the tilt angle θ of magnetic field: $\omega_c \equiv eB_z/m^*c = \omega_{c0}\cos\theta$, where B_z is the component of magnetic field perpendicular to conducting layers, e is the electron charge, m^* is the effective electron mass, and c is the light velocity. In Ref. [26] the MQOs are neglected and $\sigma_{zz} \approx \sigma_{zz}^0$, where the interlayer conductivity without magnetic field

$$\sigma_{zz}^0 = e^2\rho_F\langle v_z^2\rangle\tau = 2e^2t_z^2m^*\tau d/\pi\hbar^4, \tag{3}$$

$\rho_F = m^*/\pi\hbar^2 d$ is the three-dimensional (3D) density of states (DOS) at the Fermi level in the absence of magnetic field per two spin components, and the mean-square interlayer electron velocity along the interlayer direction is $\langle v_z^2\rangle = 2t_z^2d^2/\hbar^2$. Equation (2) agrees with the result of Yamaji at $\omega_c\tau \to \infty$. A microscopic calculation of Q2D AMROs using the Kubo formula and electron dispersion in Eq. (1), neglecting the MQOs, also gives Eq. (2) when the number of filled Landau

*Corresponding author: grigorev@itp.ac.ru

levels (LLs) $n_{LL}^F \gg 1$ [27]. The assumption $\sigma_{zz} \approx \sigma_{zz}^0$ in Eq. (2) is valid only in weak magnetic field, such that $\omega_c\tau \ll 1$, so that MQOs are negligible and AMROs are also weak. In strong magnetic field, $\omega_c\tau \gtrsim 1$, when both AMROs and MQOs are strong, Eq. (2) is, generally, incorrect.

The standard theory of MQOs and of AMROs considers these two phenomena independently, i.e., neglecting their interplay, which is valid only in the limit of weak MQOs and AMROs [2,3]. Usually, to analyze the experimental data in quasi-2D metals in the high-field limit one applies Eq. (2) with a phenomenological replacement $\sigma_{zz} = \sigma_{zz}^{\rm MQO}(B_z)$, where $\sigma_{zz}^{\rm MQO}(B_z)$ depends on magnetic field $\boldsymbol{B}$ due to only the MQOs. Then the angular and field dependences of $\sigma_{zz}(\boldsymbol{B})$ factorize:

$$\sigma_{zz}(\boldsymbol{B}) = \Phi_{\rm AMRO}(\theta)\sigma_{zz}^{\rm MQO}(B), \tag{4}$$

where $\Phi_{\rm AMRO}(\theta)$ is given by Eq. (2) and depends on the field strength B via the product $\omega_c\tau$ and $\sigma_{zz} = \sigma_{zz}^{\rm MQO}(B) = \sigma_{zz}^0 + \tilde{\sigma}_{zz}(B)$ include MQOs. The oscillating part $\tilde{\sigma}_{zz}$ of the conductivity is given by a sum of MQOs with all frequencies $F_a = S_{\rm ext}^a \hbar c/2\pi e$, determined by the Fermi surface (FS) extremal cross-section areas $S_{\rm ext}^a$ [1,2,28,29]:

$$\frac{\sigma_{zz}}{\sigma_{zz}^0} \approx \sum_a \frac{g_{0,a}}{g_{\rm tot}}\left[1 + 2\sum_{k=1}^{\infty} A_a(k)\cos\left(2\pi k\frac{F_a}{B} - \phi_a\right)\right], \tag{5}$$

where the total DOS at the Fermi level $g_{\rm tot} = \sum_a g_{0,a}$ is a sum of the contributions $g_{0,a}$ from all FS pockets a and the phase shift $\phi_a \approx \pi/4$. The MQO amplitudes $A_a(k)$ depend on the FS geometry, being also proportional to the product of three damping factors [1–3]: the Dingle factor

$$R_D(k) = \exp\left(\frac{-\pi k}{\omega_c\tau}\right), \tag{6}$$

the temperature damping factor

$$R_T(k) = \frac{2\pi^2 k_B T k/\hbar\omega_c}{\sinh(2\pi^2 k_B T k/\hbar\omega_c)}, \tag{7}$$

and the spin factor R_S, which in Q2D metals is given by [1–3]

$$R_S(k) = \cos\left(\frac{\pi k\Delta_Z}{\hbar\omega_c}\right) = \cos\left(\frac{\pi g k m^*}{2m_e\cos\theta}\right), \tag{8}$$

where the Zeeman splitting $\Delta_Z = g\hbar eB/2m_e c = gB\mu_B$ of the electron energy is independent of θ if the electron g factor g does not depend on θ [30]. In Q2D metals $\hbar\omega_c \propto \cos\theta$, and the spin factor R_S results in strong oscillating angular dependence of the MQO amplitude, given by Eq. (8), which is typical of 2D and Q2D metals and allows measuring the electron g factor from the so-called *spin zeros*, the tilt angles θ_s, where the factor in Eq. (8) becomes zero.

In Q2D metals with electron dispersion in Eq. (1) each FS pocket is a warped cylinder, giving two FS extremal cross sections. At $t_z \gg \hbar\omega_c$ the difference between these two extremal FS cross-section areas is much larger than the LL separation, and one can use the 3D formula in Eq. (5), derived in the lowest order in $\hbar\omega_c/t_z$. The simplest (but approximate at $\hbar\omega_c \sim t_z$) generalization of Eq. (5) for $\hbar\omega_c \lesssim t_z$, by analogy with the quasi-2D DOS [31], is

$$\frac{\sigma_{zz}}{\sigma_{zz}^0} \approx \sum_a \frac{g_{0,a}}{g_{\rm tot}}\left[1 + 2\sum_{k=1}^{\infty} A_a(k)\cos\left(\frac{2\pi k F_a}{B}\right)\right], \tag{9}$$

where the amplitudes

$$A_\alpha(k) = (-1)^k J_0\left(\frac{4\pi k t_z}{\hbar\omega_c}\right) R_D(k)R_T(k)R_S(k), \tag{10}$$

and the summation over α in Eq. (9) is the summation over cylindrical FS pockets rather than over FS extremal cross sections a as in Eq. (5). Note that, in contrast to Eq. (5), in Eq. (9) the phases ϕ_a are absent; in fact these phases are contained in the Bessel functions $J_0(4\pi k t_z/\hbar\omega_c)$ in the amplitudes $A_\alpha(k)$. At $\hbar\omega_c \sim t_z$ the higher-order terms in $\hbar\omega_c/t_z$ become important, and Eqs. (9) and (10) change [32–35] [see, e.g., Eqs. (18)–(21) of Ref. [34] or Eqs. (13)–(15) of Ref. [35]], producing two new physical effects: the phase shift of beats [32,34] and the slow oscillations of magnetoresistance [33,34].

When MQOs and AMROs are strong, their interplay may become essential. Then not only Eq. (2) but also Eq. (4) may be incorrect; that is, the conductivity is not simply a product of the AMRO factor in Eq. (2) and the MQO factor in Eq. (5) or (9). Recently, the influence of strong MQOs on the AMRO factor in Eq. (2) was studied [36]. It was found that in the high-field limit $\omega_c \gg 1/\tau, t_z/\hbar$ the strong MQOs modify the AMRO factor in Eq. (2), keeping the AMRO period almost untouched but changing the AMRO amplitude and its magnetic-field dependence [36]. Also the shape of LLs, which is not Lorentzian at $\omega_c \gg 1/\tau, t_z/\hbar$, is reflected in the AMRO damping. For example, for the Gaussian LL shape the terms with $\nu \neq 0$ are more strongly damped than in Eq. (2) and given by Eq. (33) of Ref. [36], which increases the AMRO amplitude. Thus, the interplay between MQOs and AMROs may be considerable at $\omega_c\tau \gg 1$.

In the present paper we study the influence of AMROs on MQOs, especially on the angular dependence of the amplitude of MQOs of magnetoresistance. We show that this influence is rather strong and, in high magnetic field, at $\omega_c \gg 1/\tau, t_z/\hbar$, may lead to a new qualitative phenomenon: the false spin zeros of MQOs of MR.

II. THE MODEL AND GENERAL FORMULAS

A. Two-layer model

To study the influence of AMROs on MQOs, we consider strongly anisotropic Q2D metals in a high magnetic field when $\omega_c \gg 1/\tau, t_z/\hbar$ and both AMROs and MQOs are strong. In this limit, to calculate the interlayer conductivity σ_{zz} one can apply the two-layer model [36–38], where σ_{zz} is calculated as a tunneling conductivity between two adjacent conducting layers using Kubo's formula with the electron Green's function taken inside the 2D conducting layer with disorder (see the Appendix). It was shown that this two-layer model is equivalent to the 3D models with strongly anisotropic electron dispersion $\epsilon_{3D}(\mathbf{k})$ if $\omega_c \gg 1/\tau, t_z/\hbar$ [39]. Then

$$\sigma_{zz}(T) = \frac{1}{2}\sum_{s=\pm1}\int d\varepsilon[-n_F'(\varepsilon)]\sigma_{zz}(\varepsilon + s\Delta_Z), \tag{11}$$

where $n'_F(\varepsilon) = -1/\{4T\cosh^2[(\varepsilon-\mu)/2T]\}$ is the derivative of the Fermi distribution function, $\mu = E_F$ is the chemical potential of the electrons, and [36]

$$\frac{\sigma_{zz}(\varepsilon)}{\sigma^0_{zz}} = \frac{2\Gamma_0\hbar\omega_c}{\pi}\sum_{n,p\in Z} Z(n,p)\mathrm{Im}G(\varepsilon,n)\mathrm{Im}G(\varepsilon,n+p). \tag{12}$$

Here the function Z comes from the overlap of electron wave functions on adjacent layers, producing AMROs, and is given by Eq. (12) of Ref. [36], which coincides with the square of Eq. (9) in Ref. [40]. The interlayer conductivity in the absence of magnetic field is given by $\sigma^0_{zz} = 2e^2\tau_0 m^* t_z^2 d/\pi\hbar^4$, and $\Gamma_0 = \hbar/2\tau_0$. Equation (12) is valid for arbitrary electron Green's functions

$$G(\varepsilon,n) = \frac{1}{\varepsilon - \hbar\omega_c(n+1/2) - \Sigma(\varepsilon)}, \tag{13}$$

which contain the self-energy part $\Sigma(\varepsilon)$ determined by disorder. Below we neglect the electron-electron ($e-e$) interaction, which can be used only when many LLs are filled, $n^F_{LL} = \lceil\mu/\hbar\omega_c\rceil \gg 1$, and the $e-e$ interaction is effectively screened [41,42]. In this limit $n^F_{LL} \gg 1$ the function $Z(n,p)$ simplifies to [27,36]

$$Z(n,p) \approx Z\left(n^F_{LL},p\right) \approx J_p^2(k_F d\tan\theta) \equiv J_p^2(\kappa). \tag{14}$$

With the notations $\Gamma(\varepsilon) = |\mathrm{Im}\Sigma(\varepsilon)| = -\mathrm{Im}\Sigma^R(\varepsilon)$ and $\varepsilon^* \equiv \varepsilon - \mathrm{Re}\Sigma(\varepsilon)$, the imaginary part of the electron Green's function is

$$\mathrm{Im}G(\varepsilon,n) = -\Gamma(\varepsilon)/\{[\varepsilon^* - \hbar\omega_c(n+1/2)]^2 + \Gamma^2(\varepsilon)\}. \tag{15}$$

Using also the notations $\varepsilon^* \equiv \varepsilon - \mathrm{Re}\Sigma(\varepsilon)$, $\gamma_0 = 2\pi\Gamma_0/\hbar\omega_c$, $\gamma \equiv 2\pi|\mathrm{Im}\Sigma(\varepsilon)|/\hbar\omega_c$, and $\alpha \equiv 2\pi\varepsilon^*/\hbar\omega_c$, from Eqs. (12)–(15) one obtains

$$\frac{\sigma_{zz}(\varepsilon)}{\sigma^0_{zz}} = \frac{\Gamma_0}{\Gamma(\varepsilon)}\sum_{p=-\infty}^{\infty} S_p[J_p(\kappa)]^2, \tag{16}$$

where

$$S_0 \equiv \sum_{n\in Z}\frac{(2/\pi)\hbar\omega_c\Gamma^3}{\left[\left(\varepsilon^* - \hbar\omega_c\left(n+\frac{1}{2}\right)\right)^2 + \Gamma^2\right]^2} = \frac{\sinh(\gamma)}{\cos(\alpha)+\cosh(\gamma)} - \gamma\frac{1+\cos(\alpha)\cosh(\gamma)}{[\cos(\alpha)+\cosh(\gamma)]^2}, \tag{17}$$

in agreement with Eq. (23) of Ref. [35], and for $p \neq 0$

$$S_p \equiv \sum_{n\in Z}\frac{(2/\pi)\hbar\omega_c\Gamma^3}{\{[\varepsilon^* - \hbar\omega_c(n+1/2)]^2+\Gamma^2\}} \times \frac{1}{\{[\varepsilon^* - \hbar\omega_c(n+p+1/2)]^2+\Gamma^2\}} = \frac{\sinh(\gamma)}{[\cos(\alpha)+\cosh(\gamma)][1+(p\pi/\gamma)^2]}. \tag{18}$$

Equations (16)–(18) give both AMROs and MQOs for arbitrary (unknown yet) electron self-energy $\Sigma(\varepsilon)$.

At $\gamma \gg 1$ (weak-field limit) the second term in Eq. (17) is exponentially small, so that S_0 in Eq. (17) is the same as S_p in Eq. (18) at $p = 0$. Hence, as expected, at $\gamma \gg 1$ we confirm Eqs. (2) and (4). However, at $\gamma \ll 1$ (high-field limit) the second term in Eq. (17) is important, and the function S_0 in Eq. (17) becomes completely different from $S_p(p=0)$ in Eq. (18). This means that at $\gamma \ll 1$ Eqs. (2) and (4) are not valid for any self-energy $\Sigma(\varepsilon)$. The difference between the functions S_0 and $S_p(p=0)$, leading to the violation of Eqs. (2) and (4), is illustrated in Fig. 1 at $|\mathrm{Im}\Sigma(\varepsilon)| = \Gamma_0 = \mathrm{const}$ and is clearly seen already from the expansions of S_0 and of $S_p(p=0)$ at $\gamma \to 0$:

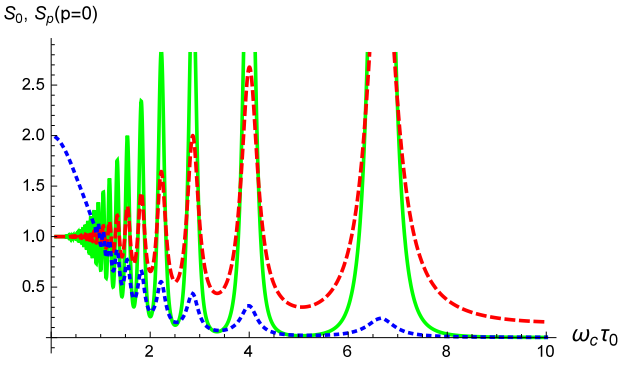

FIG. 1. Comparison of the functions $S_0(B_z)$ (solid green line) and $S_p(B_z)$ at $p=0$ (dashed red line), given by Eqs. (17) and (18) at $|\mathrm{Im}\Sigma(\varepsilon)| = \Gamma_0 = \mathrm{const}$ and $\alpha = 20\gamma$. Both functions show oscillations around the same background, but the amplitude of the oscillations of $S_0(B_z)$ is much stronger at $\gamma \ll 1$. The dotted blue line gives $2S_p(p=1)$ for comparison.

$$S_0(\gamma\to 0) = \frac{2-\cos(\alpha)}{[1+\cos(\alpha)]^2}\frac{\gamma^3}{3} + O[\gamma]^5,$$
$$S_p\Big|_{\substack{\gamma\to 0,\\ p=0}} = \frac{\gamma}{1+\cos(\alpha)} - \frac{2-\cos(\alpha)}{[1+\cos(\alpha)]^2}\frac{\gamma^3}{6} + O[\gamma]^5. \tag{19}$$

For example, in the minima of MQOs of conductivity, i.e., at $\alpha = 0$, Eq. (19) shows that the function S_0 is much smaller than $S_p(p=0)$ at $\gamma \to 0$:

$$S_0\Big|_{\substack{\gamma\to 0,\\ \alpha=0}} \approx \frac{\gamma^3}{12} \ll S_p\Big|_{\substack{\gamma\to 0,\\ p=0\\ \alpha=0}} \approx \frac{\gamma}{2}. \tag{20}$$

These expansions (19) and (20) are valid at any α except in the proximity of the point $\alpha = \pi$, where the denominator in (19) vanishes. At $\alpha = \pi$ and $\gamma \to 0$ the expansion of Eqs. (17) and (18) gives

$$S_0\Big|_{\substack{\gamma\to 0,\\ \alpha=\pi}} \approx \frac{4}{\gamma}, \quad S_p\Big|_{\substack{\gamma\to 0,\\ p=0\\ \alpha=\pi}} \approx \frac{2}{\gamma}; \tag{21}$$

that is, in the maxima of MQOs at $\gamma \to 0$ the function S_0 is only two times larger than $S_p(p=0)$.

As shown in Refs. [34,35], the function S_0 differs from $S_p(p=0)$ because of the extra term G^2_R in the Kubo formula for conductivity. This term contributes only second-order poles in the integrand over ε, which does not affect the result at zero magnetic field but contributes the term $\sim\gamma$ to the amplitudes of MQO harmonics of conductivity [34,35].

B. Electron Green's function and self-energy

Expression (13) for the electron Green's function contains the self-energy $\Sigma(\varepsilon)$, which at low temperature mainly comes from the scattering by the impurity potential

$$V_i(\mathbf{r}) = \sum_j U\delta^3(\mathbf{r} - \mathbf{r}_j). \tag{22}$$

The impurities are assumed to be short range (pointlike) and randomly distributed with volume concentration n_i. The scattering by this impurity potential is spin independent. In the noncrossing (self-consistent single-site) approximation the electron self-energy satisfies the following equation [43]:

$$\Sigma(\varepsilon) = \frac{n_i U}{1 - UG(\varepsilon)}, \tag{23}$$

where the averaged Green's function in the coinciding points [35,44]

$$G(\varepsilon) = \sum_{n,k_y,k_z} G(\varepsilon,n) = \frac{g_{LL}}{d}\sum_{n=0}^{+\infty} G(\varepsilon,n) \tag{24}$$

$$\approx \frac{g_{LL}}{d}\sum_{n=-\infty}^{+\infty} \frac{1}{\varepsilon - \hbar\omega_c(n+1/2) - \Sigma(\varepsilon)} \tag{25}$$

$$= -\frac{\pi g_{LL}}{\hbar\omega_c d}\tan\left[\pi\frac{\varepsilon - \Sigma(\varepsilon)}{\hbar\omega_c}\right]. \tag{26}$$

The summation over k_y in Eq. (24) gives the LL degeneracy $g_{LL} = eB_z/2\pi\hbar c$, and the summation over k_z gives $1/d$. Strictly speaking, in Eqs. (24) the summation over n must be cut at $n_{\max} \sim W/\hbar\omega_c$, where $W \sim \mu$ is the bandwidth, as the expression logarithmically diverges. Similarly, in Eq. (25) we extended the summation over n from $-\infty$ because the neglected difference $\sum_{n=-\infty}^{0} G(\varepsilon,n) \approx \ln(W/\mu)/\hbar\omega_c = \text{const}$ does not affect observable quantities. In the self-consistent Born approximation (SCBA), used below, the neglected difference is equivalent to the constant shift of the chemical potential.

It is convenient to use the normalized electron Green's function

$$g(\varepsilon) \equiv G(\varepsilon)\hbar\omega_c d/\pi g_{LL}. \tag{27}$$

To obtain the monotonic growth of longitudinal interlayer magnetoresistance [38,39,45] and other qualitative physical effects [36], the SCBA is sufficient, which instead of Eq. (23) gives

$$\Sigma(\varepsilon) - n_i U = n_i U^2 G(\varepsilon) = \Gamma_0 g(\varepsilon). \tag{28}$$

Here we used the fact that the zero-field level broadening is $\Gamma_0 = \pi n_i U^2 \nu_{3D} = \pi n_i U^2 g_{LL}/(d\hbar\omega_c) = \hbar/2\tau_0$. Below we also neglect the constant energy shift $n_i U$ in Eq. (28), which does not affect physical quantities such as conductivity.

Equations (26)–(28) give the equations for the Green's function $g \equiv g(\varepsilon)$,

$$\mathrm{Im}g = \frac{\sinh(\gamma_0 \mathrm{Im}g)}{\cosh(\gamma_0 \mathrm{Im}g) + \cos(\alpha)} = \frac{\gamma}{\gamma_0}, \tag{29}$$

$$\mathrm{Re}g = \frac{-\sin(\alpha)}{\cosh(\gamma_0 \mathrm{Im}g) + \cos(\alpha)}, \tag{30}$$

or the equations for the electron self-energy $\Sigma^R(\varepsilon)$,

$$\frac{\gamma}{\gamma_0} = \frac{\sinh(\gamma)}{\cosh(\gamma) + \cos(\alpha)}, \tag{31}$$

$$\delta \equiv \alpha - \frac{2\pi\varepsilon}{\hbar\omega_c} = \frac{\gamma_0 \sin(\alpha)}{\cosh(\gamma) + \cos(\alpha)}. \tag{32}$$

Here we have used the notations introduced after Eq. (15). The solution of Eq. (31) gives $\mathrm{Im}\Sigma(\alpha)$, while Eq. (32) allows us to find $\alpha(\varepsilon)$ and $\mathrm{Re}\Sigma(\varepsilon)$. The system of Eqs. (31) and (32) differs from Eq. (30) of Ref. [35] even in the absence of an electron reservoir (at $R = 0$) because in Eq. (30) of Ref. [35] the oscillating real part of the electron self-energy is neglected, which leads to a different dependence of $\sigma_{zz}(B_z)$ [39].

Equation (31) allows us to find the value γ_{0c} when the LLs become isolated in SCBA, i.e., when the DOS and $\mathrm{Im}\Sigma^R(\varepsilon)$ between LLs become zero. When the energy is in the middle between two adjacent LLs $\cos(\alpha) = 1$, and Eq. (31) for $\gamma_{\min}$ at the conductivity minima becomes

$$\frac{\gamma_{\min}}{\gamma_0} = \frac{\sinh(\gamma_{\min})}{\cosh(\gamma_{\min}) + 1} = \tanh(\gamma_{\min}/2). \tag{33}$$

This equation always has a trivial solution, $\gamma = 0$. However, at $\gamma_0 > \gamma_{0c} = 2$, corresponding to $\pi\Gamma_0 > \hbar\omega_c$, Eq. (33) also has a nonzero solution. This nonzero solution means a finite DOS at an energy between LLs; that is, at $\pi\Gamma_0 < \hbar\omega_c$ in SCBA the LLs become isolated, which affects physical observables, e.g., leads to the monotonic growth of $\sigma_{zz}(B_z)$ [44].

When the energy is in the center of a LL $\cos(\alpha) = -1$, and Eq. (31) for $\gamma_{\max}$ at the conductivity maxima becomes

$$\frac{\gamma_{\max}}{\gamma_0} = \frac{\sinh(\gamma_{\max})}{\cosh(\gamma_{\max}) - 1} = \coth(\gamma_{\max}/2). \tag{34}$$

This equation always has a nonzero solution.

Any additional Fermi-surface parts, which are not responsible for the given MQOs, create an extra DOS at the Fermi level. This additional DOS does not oscillate with the same frequency and acts as an electron reservoir [35,46,47], smearing the MQOs. This additional DOS does not oscillate at all if it comes from open Fermi-surface parts. In this case Eq. (31) changes to

$$\frac{\gamma}{\gamma_0} = \left(\frac{\sinh(\gamma)}{\cosh(\gamma) + \cos(\alpha)} + R\right)\Big/(1 + R), \tag{35}$$

similar to Eq. (24) of Ref. [35], where R is the ratio of the reservoir DOS to the average DOS of the Fermi-surface pocket responsible for MQOs.

III. INTERPLAY BETWEEN ANGULAR AND QUANTUM MAGNETIC OSCILLATIONS

The influence of MQOs on AMROs was already studied recently [36]. In this section we analyze the influence of AMROs on MQOs of interlayer conductivity using the formulas in Sec. II. As shown in Sec. II A, the violation of Eqs. (2) and (4) and new interesting effects appear only in the high-field limit $\gamma \ll 1$ and only because of the difference between the functions S_0 and $S_p(p = 0)$ given by Eqs. (17) and (18). In this section we consider two limiting cases: (i) the limit of a large electron reservoir when $\gamma \approx \text{const}$ and (ii) the limit

of a zero-electron reservoir, when there are no Fermi-surface pockets except the one responsible for MQOs.

A. Limit of a large electron reservoir and $|\mathrm{Im}\Sigma(\varepsilon)| \approx$ const

The violation of Eqs. (2) and (4) should be strongest in the minima and maxima of conductivity MQOs, where the functions S_0 and $S_p(p=0)$ are most different (see Fig. 1). Additionally, the violation of Eqs. (2) and (4) is expected to be most evident near the Yamaji angles, where the term with $p=0$ in Eq. (16) is reduced compared to the terms with $p \neq 0$.

To check how strong these deviations from Eqs. (2) and (4) are at $|\mathrm{Im}\Sigma(\varepsilon)| \approx$ const, in Fig. 2 we compare $\sigma_{zz}^{\mathrm{new}}(\varepsilon)$ calculated using Eqs. (16)–(18) and $\sigma_{zz}^{\mathrm{old}}(\varepsilon)$ calculated using Eqs. (4) and (2) and Eq. (23) of Ref. [35], i.e., $\sigma_{zz}^{\mathrm{MQO}}(B) = \sigma_{zz}^{0} S_0$. From this comparison one can see that, indeed, the notable violation of Eqs. (2) and (4) appears at $|\mathrm{Im}\Sigma(\varepsilon)| \approx$ const only near the Yamaji angles. These deviations do not change the frequency or the phase of MQOs but considerably reduce their amplitude. This decrease in MQO amplitude near the Yamaji angles compared to the prediction of Eqs. (2) and (4) is even more clear for the magnetoresistance $R_{zz} \approx 1/\sigma_{zz}$, shown in the insets in Fig. 2. Our result that at the Yamaji angles the MQO amplitude decreases contradicts the general opinion that the magnetoresistance oscillations should be stronger at the Yamaji angles because the system becomes effectively two-dimensional. Figure 2 also illustrates a strong influence of AMROs on the amplitude of MQOs.

The angular dependences of conductivity and of magnetoresistance as a function of the tilt angle θ for a constant magnetic field strength B_0, calculated using Eqs. (11) and (16)–(18), are plotted in Fig. 3 at two temperatures: $T = 0.1\Gamma_0$ (blue solid line) and $T = 0.4\Gamma_0$ (red dashed line). $E_F = 201\Gamma_0$ and $\omega_{c0}\tau_0 = 5$ at $\theta = 0$. The fast quantum oscillations come from the angular dependence of the perpendicular to layer component $B_z = B_0 \cos\theta$ of magnetic field, which enters the MQOs. According to the above analytical estimates, the amplitude of MQOs considerably decreases near the Yamaji angles, which in Fig. 3 is seen as the angular oscillations of the amplitude of MQO. In an analysis of experimental data for magnetoresistance such beats of the MQO amplitude may be mistakenly interpreted as spin zeros. We suggest the name *false spin zeros* for this phenomenon of the angular beats of MQO amplitude due to the interplay between AMROs and MQOs in quasi-2D metals. Increasing temperature damps the MQOs, but these false spin zeros are still visible.

The false spin zeros become even more pronounced if one takes into account the incoherent channels of interlayer conductivity, which come from crystal imperfections, from resonance impurities between the conducting layers [48–50], or from polaron tunneling [51,52]. The incoherent channels produce the additional term σ_{zz}^{i} for the interlayer conductivity. This term has neither angular nor quantum oscillations and shifts conductivity in Fig. 3 upward by a constant. The total conductivity is a sum of the coherent and incoherent conductivity channels: $\sigma_{zz}^{\mathrm{tot}} = \sigma_{zz}^{\mathrm{coh}} + \sigma_{zz}^{i}$. Usually, in clean metals the ratio $\sigma_{zz}^{i}/\sigma_0 \ll 1$. In Fig. 4 we plot the angular dependence of interlayer magnetoresistance $R_{zz} = 1/\sigma_{zz}^{\mathrm{tot}}$ for two different values of this ratio: $\sigma_{zz}^{i}/\sigma_0 = 0.04$ [Fig. 4(a)]

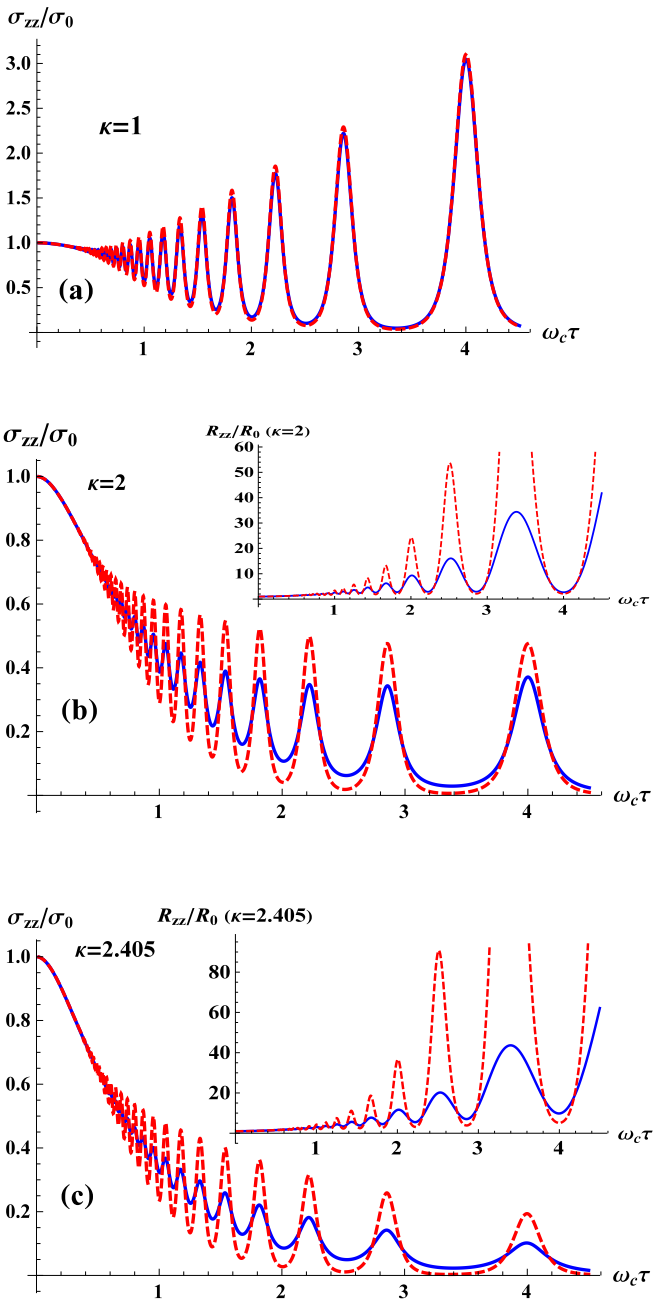

FIG. 2. Comparison of the new formula for conductivity $\sigma_{zz}^{\mathrm{new}}(B_z)$, given by Eqs. (16)–(18) and shown by the solid blue line, with $\sigma_{zz}^{\mathrm{old}}(B_z)$, given by Eqs. (4) and (2) with $\sigma_{zz}^{\mathrm{MQO}}(B) = \sigma_{zz}^{0} S_0(B_z)$ and shown by the dashed red line. For this comparison we take three different values of $\kappa \equiv k_F d \tan\theta$: (a) $\kappa_1 = 1$, (b) $\kappa_2 = 2$, and (c) $\kappa_3 = 2.405$. The latter corresponds to the first Yamaji angle. The insets show resistivity $R_{zz}(B_z) \approx 1/\sigma_{zz}(B_z)$.

and $\sigma_{zz}^{i}/\sigma_0 = 0.2$ [Fig. 4(b)]. The magnetic field strength in Fig. 4 corresponds to $\omega_{c0}\tau_0 = 5$ at $\theta = 0$ and $k_F d = 3$. The false spin zeros, seen as the angular beats of MQO amplitude, are clearer in Fig. 4 than in Fig. 3.

The long-range disorder, which has a length scale greater than the magnetic length, affects the MQO amplitude differently from the short-range disorder [40]. The macroscopic sample inhomogeneities locally shift the Fermi level and

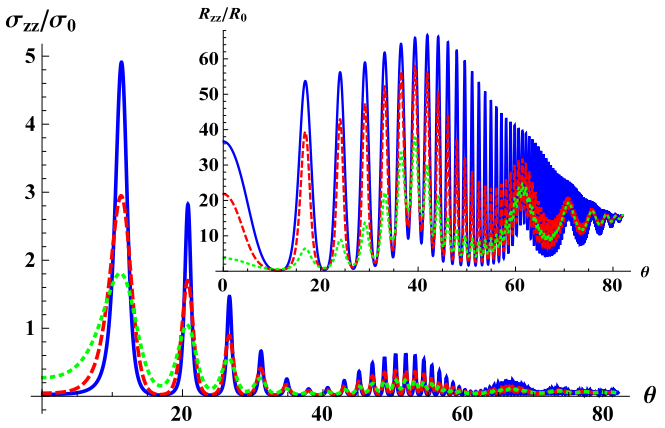

FIG. 3. The angular dependence of conductivity (main panel) and magnetoresistance (inset) at $k_F d = 3$, $\omega_{c0}\tau_0 = 5$ and at three temperatures: $T = 0.1\Gamma_0$ (blue solid line), $T = 0.5\Gamma_0$ (red dashed line), and $T = \Gamma_0$ (green dotted line). The minima of the MQO amplitude, arising from the influence of AMROs on MQOs, may be erroneously treated as spin zeros.

damp the MQOs similar to the temperature smearing of the Fermi level. However, this type of disorder keeps the AMRO amplitude unchanged, similar to the amplitude of the so-called slow oscillations of magnetoresistance [33,34]. Using these slow oscillations in organic metals, it was shown [33] that the contribution $T_D^{\rm inh}$ of such sample inhomogeneities to the total Dingle temperature T_D of MQOs exceeds more than four times the contribution T_D^* to the Dingle temperature from the short-range disorder. This information is helpful for understanding the nature of disorder in various compounds. The observation of slow oscillations requires that the Landau-level separation $\hbar\omega_c$ is less than the interlayer transfer integral t_z but exceeds the Dingle temperature, i.e., $t_z > \hbar\omega_c > \Gamma_0$. In very anisotropic compounds, where $t_z \lesssim \Gamma_0$, this condition cannot be satisfied, and the slow oscillations are very difficult to observe. However, just in this limiting case the comparison of the amplitudes of AMROs and MQOs allows us to determine the contribution $T_D^{\rm inh}$ of these sample inhomogeneities from experimental data on magnetoresistance because the amplitude of AMROs is not affected by $T_D^{\rm inh}$, contrary to the amplitude of MQOs. The observation of false spin zeros in the amplitude of MQOs and their temperature evolution increases the accuracy of such an extraction of various contributions to the Dingle temperature from experimental data.

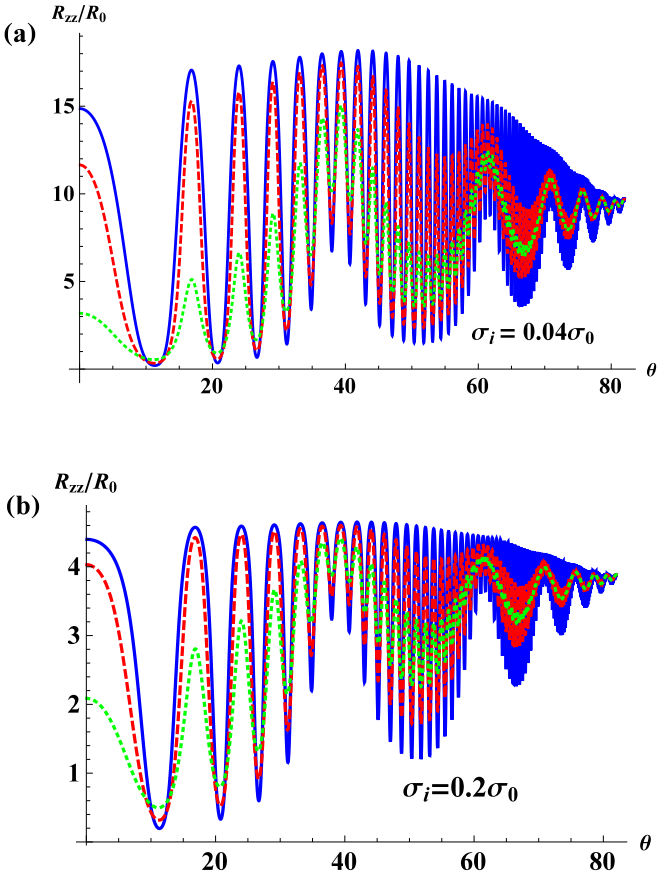

FIG. 4. The angular dependence of magnetoresistance in the presence of the incoherent channel of interlayer conductivity at (a) $\sigma_{zz}^i = 0.04\sigma_0$ and (b) $\sigma_{zz}^i = 0.2\sigma_0$ for three temperatures: $T = 0.1\Gamma_0$ (blue solid line), $T = 0.5\Gamma_0$ (red dashed line), and $T = \Gamma_0$ (green dotted line).

B. Conductivity in the absence of an electron reservoir

In the absence of an electron reservoir the electron Green's function and self-energy are given by Eqs. (29)–(32). In this limit, to calculate conductivity one needs to solve the self-consistency equation (31) for the self-energy, which can be done only numerically. In the minima and maxima of MQOs of conductivity Eq. (31) simplifies to Eqs. (33) and (34), respectively, which are convenient to calculate the envelope of MQOs, shown in Fig. 5 for $k_F d = 3$ and $\gamma_0 = \pi/\omega_c\tau_0 = 2$. In Fig. 6 we plot the normalized amplitude of MQOs of conductivity $(\sigma_{zz}^{\max} - \sigma_{zz}^{\min})/\sigma_0$ for $k_F d = 3$ and for various

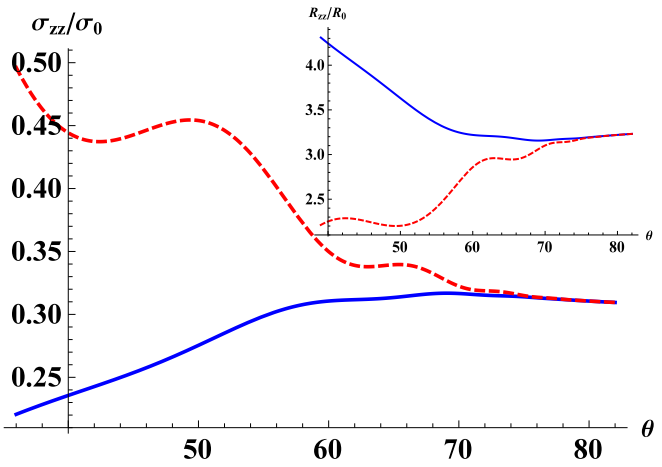

FIG. 5. The maxima (solid blue line) and minima (dashed red line) of quantum oscillations of interlayer conductivity (main panel) and of magnetoresistance (inset) calculated in SCBA in the absence of an electron reservoir as a function of the tilt angle θ of the magnetic field at $k_F d = 3$ and $\gamma_0 = 2$. These plots give the angular dependence of the envelope of MQOs.

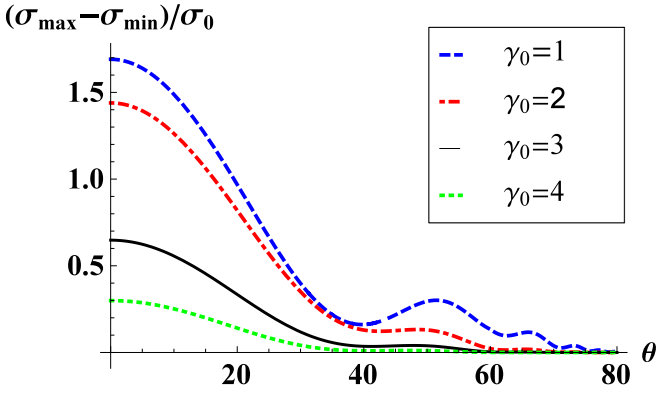

FIG. 6. Angular dependence of the relative amplitude $(\sigma_{zz}^{max} - \sigma_{zz}^{min})/\sigma_0$ of the oscillations of interlayer conductivity at $k_F d = 3$ for various γ_0 calculated in SCBA in the absence of an electron reservoir.

values of γ_0. In Fig. 7 we plot the normalized amplitude of MQOs of conductivity $(\sigma_{zz}^{max} - \sigma_{zz}^{min})/\sigma_0$ for $\gamma_0 = 3$ and for various values of $k_F d$. These plots show that the false spin zeros are more pronounced at larger $k_F d$, when AMROs are faster, and are more easily observed at $\gamma_0 < 4$. Note that in both limiting cases, i.e., for large and zero-electron reservoirs, the proposed false spin zeros only decrease the amplitude of MQOs and do not produce the phase inversion of MQOs. Thus, in contrast to true spin zeros, given by the factor R_s in Eq. (8), which changes sign and thus leads to the phase shift of MQOs by π, the false spin zeros are not strong enough to make such an inversion of MQOs. This difference can be used to distinguish between the true and false spin zeros in experimental data.

IV. CONCLUSIONS

In this paper we analyzed the influence of the AMROs in quasi-2D metals on quantum oscillations. We showed that the previous assumption of factorization of these two types of oscillations, given by Eq. (4) and usually applied to analyze experimental data, is violated in high magnetic field when $\omega_c\tau \gtrsim 1$. The strongest violation of Eq. (4) is near the Yamaji angles (AMRO maxima), where the amplitude of MQOs is strongly reduced. This interplay of AMROs and MQOs at $\omega_c\tau \gtrsim 1$ leads to the new qualitative effect: the oscillations (beats) of the amplitude of MQOs as a function of the tilt angle θ of the magnetic field. These angular minima of the MQO amplitude, originating from AMROs and called false spin zeros, may be erroneously treated as true spin zeros and lead to the incorrect determination of the electron g factor from MQOs. The proposed false spin zeros do not produce the phase inversion of MQOs and thus can be distinguished from the true spin zeros. The false spin zeros are more pronounced at larger values of $\omega_c\tau$ (see Fig. 6) and at larger values of $k_F d$, where AMROs have larger frequency (see Fig. 7). The incoherent channels of interlayer conductivity also make the proposed effect of false spin zeros stronger, which is seen from the comparison shown in Figs. 3 and 4. The false spin zeros may help to determine the contribution of such an incoherent channel to the total interlayer conductivity from experimental data. The comparison of the amplitudes of angular and quantum oscillations may help to determine the nature of the disorder which contributes to the Dingle temperature.

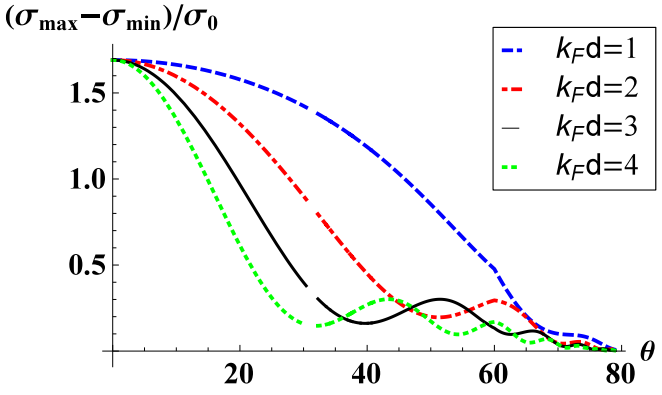

FIG. 7. Angular dependence of the relative amplitude $(\sigma_{zz}^{max} - \sigma_{zz}^{min})/\sigma_0$ of oscillations of interlayer conductivity for various $k_F d$ at $\gamma_0 = 3$ calculated in SCBA.

ACKNOWLEDGMENTS

The authors are grateful to T. Ziman for useful discussions. P.D.G. acknowledges financial support from Russian Science Foundation (Project No. 16-42-01100), and T.I.M. acknowledges support from RFBR Grant No. 16-02-00522.

APPENDIX: THE TWO-LAYER MODEL

In this appendix we recall the formulation and basic formulas of the two-layer model for interlayer conductivity, developed in Refs. [36–38]. The one-electron Hamiltonian in layered metals with small interlayer coupling consists of the three terms:

$$\hat{H} = \hat{H}_0 + \hat{H}_t + \hat{H}_I. \quad \text{(A1)}$$

The first term, $\hat{H}_0$, is the 2D free-electron Hamiltonian summed over all layers j and all quantum numbers $\{m\}$ of electrons in the magnetic field on a 2D conducting layer:

$$\hat{H}_0 = \sum_{m,j} \epsilon_{2D}(m) c^+_{m,j} c_{m,j},$$

where $\epsilon_{2D}(m) = \epsilon_n = \hbar\omega_c(n + 1/2)$ is the corresponding free-electron dispersion and c^+_m (c_m) are the electron creation (annihilation) operators in state $\{m\}$. The second term in Eq. (A1) gives the coherent electron tunneling between two adjacent layers:

$$\hat{H}_t = 2t_z \sum_j \int d^2\boldsymbol{r} [\Psi^\dagger_j(\boldsymbol{r})\Psi_{j-1}(\boldsymbol{r}) + \Psi^\dagger_{j-1}(\boldsymbol{r})\Psi_j(\boldsymbol{r})], \quad \text{(A2)}$$

where $\Psi_j(x,y)$ and $\Psi^\dagger_j(x,y)$ are the creation and annihilation operators of an electron on layer j at the point (x,y). This interlayer tunneling Hamiltonian is called "coherent" because it conserves the in-plane electron momentum during the interlayer tunneling. The last term, $\hat{H}_I$, is the impurity potential $V_i(\mathbf{r})$, e.g., given by Eq. (22).

In the strongly anisotropic almost 2D limit, $t_z \ll \Gamma, \hbar\omega_c$, the interlayer hopping t_z can be considered a perturbation for the periodic stack of uncoupled 2D metallic layers. The interlayer conductivity σ_{zz}, associated with the Hamiltonian (A2), can be calculated using the Kubo formula as the tunneling conductivity between two adjacent conducting layers j and $j+1$ [37,38]:

$$\sigma_{zz} = \frac{4e^2 t_z^2 d}{\pi\hbar} \int d\varepsilon [-n_F'(\varepsilon)] \times \int d^2\boldsymbol{r} \langle \mathrm{Im}G(\boldsymbol{r}, j, \varepsilon)\rangle \langle \mathrm{Im}G(-\boldsymbol{r}, j+1, \varepsilon)\rangle, \quad \text{(A3)}$$

where the electron Green's function $G(\boldsymbol{r}, j, \varepsilon)$ on the metallic layer j includes the scattering by impurities. The angular brackets in Eq. (A3) mean averaging over impurity configurations. Assuming the impurity distributions on adjacent layers are uncorrelated, the impurity averaging for each Green's function in Eq. (A3) is performed independently [53]. Then the averaged Green's function depends only on the difference $\boldsymbol{r}$ between the two coordinates: $\langle G(\boldsymbol{r}_1, \boldsymbol{r}_2, j, \varepsilon)\rangle = \langle G(\boldsymbol{r}, j, \varepsilon)\rangle$, where $\boldsymbol{r} = \boldsymbol{r}_2 - \boldsymbol{r}_1$.

The AMROs of interlayer conductivity in Eq. (A3) appear because in a magnetic field $B = (B_x, 0, B_z) = (B\sin\theta, 0, B\cos\theta)$, tilted by the angle θ of the normal to conducting layers, the Green's functions on two adjacent layers acquire a phase shift [see Eq. (49) of Ref. [37]]:

$$G_R(\boldsymbol{r}, j+1, \varepsilon) = G_R(\boldsymbol{r}, j, \varepsilon) \exp\{ie\Lambda(\boldsymbol{r})/\hbar\}, \quad \text{(A4)}$$

where

$$\Lambda(\boldsymbol{r}) = -yB_x d = -yBd\sin\theta. \quad \text{(A5)}$$

In the so-called "noncrossing" approximation, where the electron self-energy contains only diagrams without intersections of impurity lines, the averaged Green's function of each layer factorizes to (see the Appendix in Ref. [38] for the proof)

$$G(\boldsymbol{r}_1, \boldsymbol{r}_2, \varepsilon) = \sum_{n,k_y} \Psi^{0*}_{n,k_y}(\boldsymbol{r}_2)\Psi^{0}_{n,k_y}(\boldsymbol{r}_1) G(\varepsilon, n). \quad \text{(A6)}$$

Then the integration over $\boldsymbol{r}$ in Eq. (A3) can be performed analytically and gives [36] Eqs. (12) and (14).

[1] D. Shoenberg, *Magnetic Oscillations in Metals* (Cambridge University Press, Cambridge, 1984).
[2] A. A. Abrikosov, *Fundamentals of the Theory of Metals* (North-Holland, Amsterdam, 1988).
[3] J. M. Ziman, *Principles of the Theory of Solids* (Cambridge University Press, Cambridge, 1972).
[4] M. V. Kartsovnik, P. A. Kononovich, V. N. Laukhin, and I. F. Shchegolev, Pis'ma Zh. Eksp. Teor. Fiz. **48**, 498 (1988) [JETP Lett. **48**, 541 (1988)].
[5] K. Yamaji, J. Phys. Soc. Jpn. **58**, 1520 (1989).
[6] M. V. Kartsovnik, Chem. Rev. **104**, 5737 (2004).
[7] J. Singleton, Rep. Prog. Phys. **63**, 1111 (2000).
[8] M. V. Kartsovnik and V. G. Peschansky, Fiz. Nizk. Temp. (Kharkov) **31**, 249 (2005) [Low Temp. Phys. **31**, 185 (2005)].
[9] T. Ishiguro, K. Yamaji, and G. Saito, *Organic Superconductors*, 2nd ed. (Springer, Berlin, 1998).
[10] J. Wosnitza, *Fermi Surfaces of Low-Dimensional Organic Metals and Superconductors* (Springer, Berlin, 1996).
[11] J. S. Brooks, V. Williams, E. Choi, D. Graf, M. Tokumoto, S. Uji, F. Zuo, J. Wosnitza, J. A. Schlueter, H. Davis, R. W. Winter, G. L. Gard, and K. Storr, New J. Phys. **8**, 255 (2006).
[12] *The Physics of Organic Superconductors and Conductors*, edited by A. G. Lebed, Springer Series in Materials Science Vol. 110 (Springer, Berlin, 2008).
[13] M. Kuraguchi, E. Ohmichi, T. Osada, and Y. Shiraki, Synth. Met. **133–134**, 113 (2003).
[14] C. Bergemann, A. P. Mackenzie, S. R. Julian, D. Forsythe, and E. Ohmichi, Adv. Phys. **52**, 639 (2003).
[15] U. Beierlein, C. Schlenker, J. Dumas, and M. Greenblatt, Phys. Rev. B **67**, 235110 (2003).
[16] N. E. Hussey, M. Abdel-Jawad, A. Carrington, A. P. Mackenzie, and L. Balicas, Nature (London) **425**, 814 (2003).
[17] M. Abdel-Jawad, M. P. Kennett, L. Balicas, A. Carrington, A. P. Mackenzie, R. H. McKenzie, and N. E. Hussey, Nat. Phys. **2**, 821 (2006).
[18] M. Abdel-Jawad, J. G. Analytis, L. Balicas, A. Carrington, J. P. H. Charmant, M. M. J. French, and N. E. Hussey, Phys. Rev. Lett. **99**, 107002 (2007).
[19] M. P. Kennett and R. H. McKenzie, Phys. Rev. B **76**, 054515 (2007).
[20] M. V. Kartsovnik, T. Helm, C. Putzke, F. Wolff-Fabris, I. Sheikin, S. Lepault, C. Proust, D. Vignolles, N. Bittner, W. Biberacher, A. Erb, J. Wosnitza, and R. Gross, New J. Phys. **13**, 015001 (2011).
[21] S. K. Lewin and J. G. Analytis, Phys. Rev. B **92**, 195130 (2015).
[22] M. V. Kartsovnik, V. N. Laukhin, S. I. Pesotskii, I. F. Schegolev, and V. M. Yakovenko, J. Phys. I (France) **2**, 89 (1992).
[23] M. S. Nam, S. J. Blundell, A. Ardavan, J. A. Symington, and J. Singleton, J. Phys. Condens. Matter **13**, 2271 (2001).
[24] C. Bergemann, S. R. Julian, A. P. Mackenzie, S. NishiZaki, and Y. Maeno, Phys. Rev. Lett. **84**, 2662 (2000).
[25] P. D. Grigoriev, Phys. Rev. B **81**, 205122 (2010).
[26] R. Yagi, Y. Iye, T. Osada, and S. Kagoshima, J. Phys. Soc. Jpn. **59**, 3069 (1990).
[27] Y. Kurihara, J. Phys. Soc. Jpn. **61**, 975 (1992).
[28] In Q2D metals with dispersion in Eq. (1) and $t_z \sim \hbar\omega_c$ the interlayer conductivity σ_{zz} in addition to MQOs has so-called slow oscillations [29,33,34,54] with frequency $F_{\mathrm{slow}} = 4t_z m^* c/e\hbar$ determined by the interlayer hopping integral t_z rather than the FS cross-section area.
[29] P. D. Grigoriev, M. M. Korshunov, and T. I. Mogilyuk, J. Supercond. Nov. Magn. **29**, 1127 (2016).
[30] The electron g factor in metals may differ from the free-electron g factor $g \approx 2$ because of electron interaction, and in nonmagnetic compounds the g factor is almost independent of θ.
[31] V. M. Gvozdikov, Fiz. Tverd. Tela (Leningrad) **26**, 2574 (1984) [Sov. Phys. Solid State **26**, 1560 (1984)]; T. Champel and V. P. Mineev, Philos. Mag. B **81**, 55 (2001).
[32] P. D. Grigoriev, M. V. Kartsovnik, W. Biberacher, N. D. Kushch, and P. Wyder, Phys. Rev. B **65**, 060403(R) (2002).

[33] M. V. Kartsovnik, P. D. Grigoriev, W. Biberacher, N. D. Kushch, and P. Wyder, Phys. Rev. Lett. **89**, 126802 (2002).
[34] P. D. Grigoriev, Phys. Rev. B **67**, 144401 (2003).
[35] T. Champel and V. P. Mineev, Phys. Rev. B **66**, 195111 (2002).
[36] P. D. Grigoriev and T. I. Mogilyuk, Phys. Rev. B **90**, 115138 (2014).
[37] P. Moses and R. H. McKenzie, Phys. Rev. B **60**, 7998 (1999).
[38] P. D. Grigoriev, Phys. Rev. B **83**, 245129 (2011).
[39] P. D. Grigoriev, Phys. Rev. B **88**, 054415 (2013).
[40] M. E. Raikh and T. V. Shahbazyan, Phys. Rev. B **47**, 1522 (1993).
[41] I. V. Kukushkin, S. V. Meshkov, and V. B. Timofeev, Usp. Fiz. Nauk **155**, 219 (1988) [Sov. Phys. Usp. **31**, 511 (1988)].
[42] I. L. Aleiner and L. I. Glazman, Phys. Rev. B **52**, 11296 (1995). Even in the limit $n_{LL}^F \gg 1$, when the *e-e* interaction is screened, it affects the g factor.
[43] T. Ando, J. Phys. Soc. Jpn. **36**, 1521 (1974).
[44] A. D. Grigoriev and P. D. Grigoriev, Low Temp. Phys. **40**, 367 (2014).
[45] P. D. Grigoriev, JETP Lett. **94**, 47 (2011).
[46] P. Grigoriev, Zh. Eksp. Teor. Fiz. **119**, 1257 (2001) [Sov. Phys. JETP **92**, 1090 (2001)].
[47] T. Champel, Phys. Rev. B **64**, 054407 (2001).
[48] A. A. Abrikosov, Phys. C (Amsterdam, Neth.) **317–318**, 154 (1999).
[49] D. B. Gutman and D. L. Maslov, Phys. Rev. Lett. **99**, 196602 (2007); Phys. Rev. B **77**, 035115 (2008).
[50] M. V. Kartsovnik, P. D. Grigoriev, W. Biberacher, and N. D. Kushch, Phys. Rev. B **79**, 165120 (2009).
[51] U. Lundin and R. H. McKenzie, Phys. Rev. B **68**, 081101(R) (2003).
[52] A. F. Ho and A. J. Schofield, Phys. Rev. B **71**, 045101 (2005).
[53] The separate averaging of the spectral functions in Eq. (A3) also assumes the neglect of vertex corrections [55] in the Kubo formula. The vertex corrections to the interlayer conductivity in Eq. (A3) are negligibly small because they contain the product of the electron wave functions on adjacent layers, which is small by the factor $\sim t_z/E_F \ll 1$. In normal 3D metals the vertex corrections on pointlike impurities also vanish; they lead to the replacement of the mean scattering time τ by the transport mean scattering time [55], and these two times coincide for scattering on pointlike impurities.
[54] A. A. Sinchenko, P. D. Grigoriev, P. Monceau, P. Lejay, and V. N. Zverev, J. Low Temp. Phys. **185**, 657 (2016); P. D. Grigoriev, A. A. Sinchenko, P. Lejay, A. Hadj-Azzem, J. Balay, O. Leynaud, V. N. Zverev, and P. Monceau, Eur. Phys. J. B **89**, 151 (2016).
[55] G. Mahan, *Many-Particle Physics*, 2nd ed. (Plenum, New York, 1990).